

Static and Dynamic Contact Angle of Water Influenced by Femtosecond Laser Based Ripple Structures on Metals

Stefan Rung¹, Simon Schwarz¹, Julian Zettl¹, Babette Götzendorfer¹, Cemal Esen² and Ralf Hellmann¹

¹ Applied Laser and Photonics Group, University of Applied Sciences Aschaffenburg,
Wuerzburger Strasse 45, 63743 Aschaffenburg, Germany
E-mail: Stefan.rung@h-ab.de

² Applied Laser Technologies, Ruhr- University Bochum, Universitaetsstrasse 150, Bochum 44801,
Germany

We report on the static and dynamic contact angle on stainless steel after applying laser induced periodic surface structures and study the influence of applied femtosecond laser fluence and pulse overlap hereupon. In particular, we focus on the temporal evolution of the static contact angle, the advancing and receding contact angle, as well as on the contact angle hysteresis over a period of weeks. While directly after the generation of laser induced periodic surface structures small static contact angles and a small contact angle hysteresis are found, both properties increase after a storage of the structured specimen under ambient conditions. Particularly, the structured steel surface wettability turns into a hydrophobic regime on this time scale.

DOI: 10.2961/jlmn.2018.02.0009

Keywords: laser-induced periodic surface structures, wettability, contact angle hysteresis

1. Introduction

Adding any surface functionality by coating processes such as, e.g., spin and dip coating, chemical or physical vapor deposition is an attractive and frequently employed technical approach to tune part properties and to control the interaction of different materials with their environment. An innovative approach of such surface functionalization is laser based surface structuring using short or ultrashort pulsed lasers. Especially the application of laser induced periodic surface structures (LIPSS) by pico- and femtosecond laser enables extended surface functions in combination with a gentle surface treatment, spatial selectivity and the possibility to combine several processing steps with the same laser system (e.g. micro structuring, drilling or cutting). The generation of different categories of LIPSS like low spatial frequency LIPSS (LSFL), high spatial frequency LIPSS (HSFL) or cone like protrusions (CLP) is the focus of many research groups with the aim to fabricate these structures on all kind of materials [1].

In this study, we focus on the application of LSFL, which occur on metals, semiconductors and dielectrics after irradiation by linear polarized ultrashort laser pulses. The origin of LSFL is, generally, explained by an interference effect of the incident laser light and a surface electro-magnetic wave generated by a laser induced surface plasmon polariton (SPP). Due to this origin, LSFL occur with a spatial periodicity in the range of the employed laser wavelength and an orientation perpendicular to the polarization of the impinging laser. Several research groups have shown that LSFL properties like spatial period, orientation and homogeneity can be controlled by the applied laser fluence [2; 3], pulse to pulse overlap [4] and initial surface roughness of the solid material [5]. After the generation of LSFL, the structured

surfaces reveal two distinct modifications, namely a topographical modulation and a surface chemical modification, both affecting their potential applications.

One of the peculiar consequences on periodically structured surfaces is the alteration of their wettability, which indeed is influenced by both the morphology of the structured surface and its chemical properties. There are fundamentally three different states of wetting behavior differentiated with respect to the static contact angle (Θ_S), namely the hydrophilic ($\Theta_S < 90$), the hydrophobic ($\Theta_S > 90$) and the superhydrophobic ($\Theta_S > 150$) state.

From an application point of view, the information about the static contact angle is, however, in most cases insufficient for an advanced surface engineering. Hence, here we study for LSFL structured stainless steel surfaces the advancing contact angle (Θ_A) of a droplet with increasing drop volume and the receding contact angle (Θ_R) of a droplet with decreasing drop volume, as well as the contact angle hysteresis, i.e. the difference between the advancing and receding contact angle. Particularly the contact angle hysteresis plays an important role in industrial applications including immersion lithography, fiber coating and ink-jet printing [6].

Regarding to Young's equation (1), the contact angle of a perfectly flat surface is defined by the interfacial tension between solid/gas (σ_{sg}), solid/liquid (σ_{sl}) and liquid/gas (σ_{lg}) of the involved media.

$$\cos(\Theta_Y) = \frac{\sigma_{sg}}{\sigma_{sl} + \sigma_{lg}} \quad (1)$$

The influence of the surface roughness upon the apparent contact angle can be explained by the Wenzel state and the Cassie-Baxter state. Regarding Wenzel [7], the inherent wettability of a surface will be enhanced by the surface

roughness (see also equation (2)). Increased roughness will decrease the static contact angle on an inherently hydrophilic surface and will increase the static contact angle on an inherently hydrophobic surface. This is based on the assumption that the entire surface is wetted, i.e., there is no air gap between the surface and the liquid. In the Wenzel equation, the ratio between the wetted surface and the projected surface is defined as the parameter r .

$$\cos(\theta_s) = r \cos(\theta_Y) \quad (2)$$

Quite the contrary, the Cassie-Baxter state describes an inhomogeneous wetting taking place, as being described by air trapped in the valleys of a structured and rough surface, i.e. the liquid drop rests on a composite surface of solid and air [8]. For the calculation of the static contact angle regarding to Cassie-Baxter, the fraction of wet/solid beneath the liquid drop, defined as f , and the roughness ratio of the wetted area r has to be estimated.

$$\cos(\theta_s) = f r \cos(\theta_Y) + f - 1 \quad (3)$$

Femtosecond laser surface structuring with LIPSS modifies both the roughness and the surface chemistry, which in turn both alter the influencing factors of the Wenzel and the Cassie-Baxter state. For example, LSFL on brass increased the surface area by 40% ($r = 1.4$) and additionally triggered metal oxidation as reported in Ref. [9].

Furthermore, several groups have shown that the wetting behavior of laser structured metal surfaces significantly changes over time after the laser treatment [10–16]. Directly after irradiation, the static contact angle drops into the hydrophilic regime and increases over time to the hydrophobic regime, which is mainly attributed to a highly chemical reactive surface directly after laser treatment and a growing passive hydrophobic layer rich on carbon from the decomposition of CO_2 [17; 18]. According to Young's equation (1), the surface chemistry modification, triggered by the laser process, has an impact on the general wettability of the surface. The topographical modification introduced by laser based micro and nanostructures emphasizes the wettability change according to equation 2 and 3.

2. Experimental

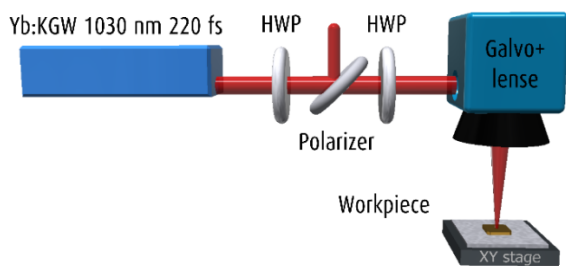


Fig. 1 Schematic laser system setup with Light Conversion Pharos 10-600. The half wave plate (HWP) and the polarizer allow precise energy adjustment; the HWP additionally controls the orientation of the laser-induced periodic surface structures.

For the experimental study we use a micro-machining station (MM200 USP, Optec SA) equipped with a 1030 nm

ultrashort pulsed laser (Pharos 10-600-PP, Light Conversion) having a pulse duration of 220 fs (FWHM) at a repetition rate of 500 kHz. Fig. 1 schematically shows the experimental setup. The applied laser pulse energy was adjusted by an external attenuator based on a rotating wave plate and a polarizer. With a half wave plate in front of the focusing unit, the linear polarization of the laser beam was also rotated orthogonally to the onwards used scanning direction. A galvo scanner (RTA AR800, Newson) was used in combination with a telecentric lens ($f = 100$ mm) to focus the beam onto the sample with a spot diameter of $36 \mu\text{m}$ ($1/e^2$). LSFL were generated on flat stainless steel (X5CrNi18-10).

The geometrical dimensions of LSFL were captured via optical light microscopy (DM6000 M, Leica Microsystems) with subsequently image analysis via 2D Fourier transformation. As it is shown in Fig. 2, this approach figures the spatial frequency, the orientation, and the homogeneity of the generated LIPSS [19].

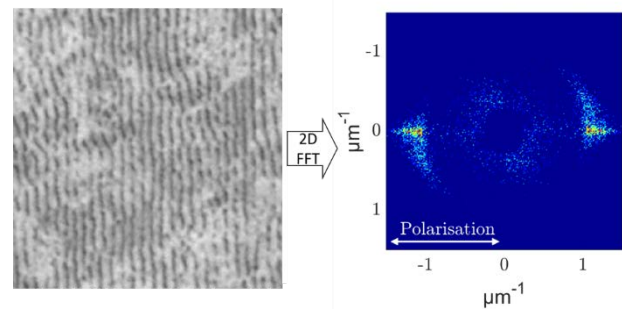


Fig. 2 Microscopy image of LSFL on stainless steel and corresponding transformed 2D Fourier spectra for the analysis of LSFL generated using a laser fluence of 0.4 J/cm^2 and a pulse overlap of 75%.

The wetting behavior was investigated using a contact angle measurement system (OCA 25, Data Physics). For the static contact angle measurement, a droplet ($6 \mu\text{L}$) of distilled water with a surface tension of 74 mN/m was deposited on the examined surface. A camera captures the droplet directly after deposition on the surface via the sessile drop method. The resulting image was analyzed to determine the apparent contact angle by circular shape fitting of the drop. For the evaluation of the dynamic contact angle, a sessile drop method with increasing and decreasing droplet volume (c.f. Fig. 3) is used to measure the advancing and receding contact angle [6]. A water volume of $10 \mu\text{L}$ is firstly add and afterwards removed using a dosing rate of $0.3 \mu\text{L/s}$. A CCD camera captures the video sequence of the extension and following contraction of the droplet. The advancing and receding contact angle are measured frame by frame and calculated by a tangential fit. The measurement system also provides information regarding the contact area between the drop and the surface. This value is necessary for the calculation of the advancing and receding contact angle. As long as the contact area increases (drop extension), the values of the contact angle measurement are taking into account for the calculation. The mean of these values represents the advancing contact angle. During the contraction, i.e. the drop volume decreases, the contact angle decreases. Once the contact area decreases, the liquid starts to de-wet the surface. The

mean of the following contact angle values represents the receding contact angle.

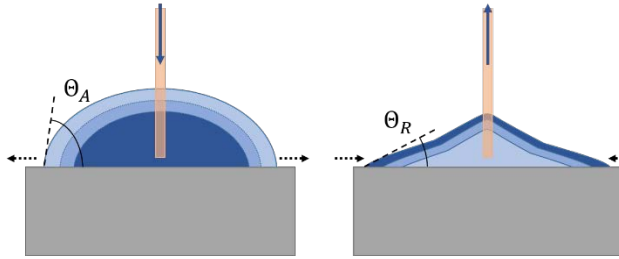


Fig. 3 Sessile drop measurement method for advancing and receding contact angle with increasing (left) and decreasing drop volume (right).

Studies by Kietzig et al. [20] and Martínez-Calderon et al. [11] have shown that the static contact angle of water on laser-structured surfaces depends on the elapsed time between the structuring process itself and the actual measurement. Until the apparent contact angle was measured, all samples were stored under ambient air at a temperature of 23 °C.

3. Results and discussion

3.1 LSFL generation

In a first step of the study, the generation of homogeneous LSFL covering a sufficiently large area to deposit liquid drops for the contact angle measurements is studied. To achieve regular two-dimensional LSFL coverage, the scanning direction is set orthogonal to the polarization of the laser light, which ensures improved connection of one-dimensional LSFL between individual scanning tracks [21]. The influence of the laser fluence and the pulse to pulse overlap on the LSFL generation is evaluated by the 2D FFT method. While the laser fluence is varied between 0.2 J/cm² and 0.8 J/cm², the pulse overlap is investigated in a range of 70% to 85% i.e. a spatial pulse to pulse distance of 10.8 μm to 5.4 μm. Please note that for a homogenous energy deposition, the given overlap represents both the consecutive laser pulse overlap within a single scanning track and the overlap between scanning tracks, i.e. the spatial distance between the deposited pulses equals the hatch pitch of the structured surface area.

All investigated processing parameters lead to a complete LSFL coverage on the stainless steel surface. The general morphology is similar to the structures in Fig 2. Rung et al. [9] determine a $|\sin(x)|$ - like surface profile description of LSFL on brass using an AFM measurement. Fig. 4 shows the resulting spatial period of LSFL on stainless steel. The inverse value of the 2D FFT centroid is plotted against the laser fluence for pulse overlap values of 70%, 75%, 80% and 85%, respectively. Apparently, with increasing laser fluence and increasing pulse overlap, the spatial period of LSFL decreases. This behavior can be explained by the induction of a surface plasma wave through the parametric decay of laser light [3] and a feedback mechanism based on a grating assisted SPP excitation and the incident laser radiation [4]. According to a previous study of Rung et al. [9], beside the spatial period also the modulation depth of LSFL increases with increasing laser fluence and pulse overlap. Both effects lead

to an increased roughness ratio (c.f. equation 2 and 3), influencing the wetting behavior according to Wenzel and Cassie-Baxter.

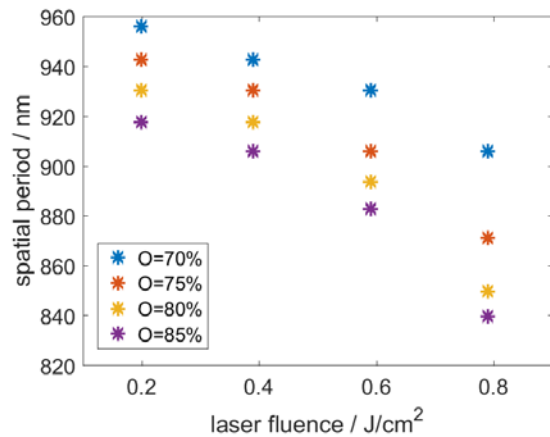


Fig. 4 Spatial period of LSFL for different pulse overlap values as a function of the laser fluence.

3.2 Static wetting behavior

Fig. 5 shows the static contact angle as a function of laser fluence directly after LSFL generation (blue line) and after a storage time of 28 days (orange line). In this diagram, the influence of the pulse overlap is represented by the error bars of each data set.

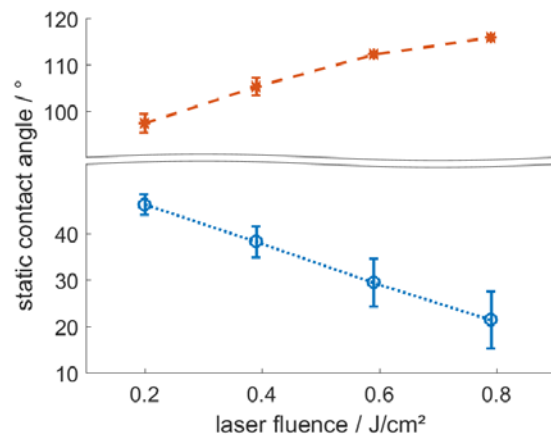


Fig. 5 Static contact angle directly after surface generation (blue) and at steady state after 4 weeks storage time (orange). Error bars represent the influence of the pulse overlap.

For applying a water droplet with a volume of 6 μL to a clean stainless steel surface without laser generated structures, a static contact angle of 68° occurs. Directly after laser irradiation, the surface reveals a hydrophilic character, i.e. a decreased static contact angle, an effect that is more pronounced for higher laser fluence. According to Fig. 5, the static contact angle θ_S drops to values between 46° for a laser fluence of 0.2 J/cm² and 21° for a laser fluence of 0.8 J/cm². After 28 days under ordinary laboratory storing conditions (ambient air and 23°C), θ_S increases and reaches a steady state between 97° for 0.2 J/cm² and 116° for 0.8 J/cm². During the storage time, the laser generated topography stays constant. According to Kietzig et al. [17] and van Ta et al., [18] this leads to the assumption, that the chem-

ical properties change over time and this change can be attributed for the temporal evolution. It is worthwhile to note, that the laser parameters which generates the lowest static contact angle directly after laser irradiation also lead to the highest contact angle in the steady state.

3.3 Dynamic wetting behavior

To evaluate the impact of LSFL and the used laser parameter onto the dynamic wetting behavior, measurements of the advancing and receding contact angle are performed. The drop volume for extension and contraction is set to 10 μL . Fig. 6 depicts the advancing contact angle θ_A during the drop expansion on the LSFL covered surface directly after the laser process. For an unstructured surface, a reference value of θ_A of $77.9^\circ \pm 1.6^\circ$ is determined. Like the static contact angle, θ_A decreases below the reference value right after LSFL generation. Similar to θ_S , increasing fluence and pulse overlap results in a further decrease of θ_A . However, advancing contact angles generated by a given laser parameter are slightly higher than those of the static contact angle, an observation that was previously reported by Eral et al. [6].

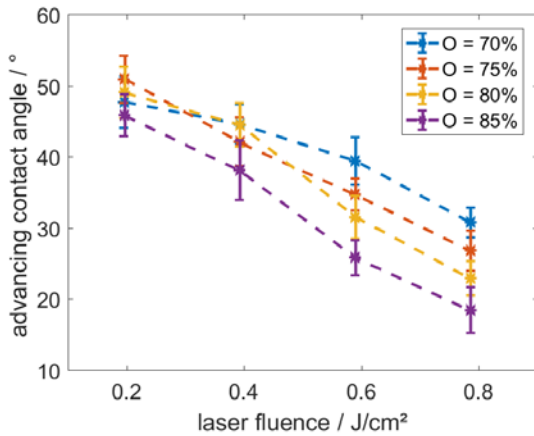


Fig. 6 Advancing contact angle directly after LSFL generation against laser fluence for different pulse overlap values.

Contrary to θ_S and θ_A , we find only a diminutive influence of the laser fluence and pulse overlap on the receding contact angle θ_R , as shown in Fig. 7. Though compared to the reference surface with θ_R being $21.3^\circ \pm 3.6^\circ$ we again find a decrease of θ_R upon LSFL structuring, the receding angle varies only slightly between 6° for 0.2 J/cm^2 and 4.5° for 0.8 J/cm^2 .

After storage time of 28 days at normal laboratory conditions, the surface reveals a hydrophobic characteristic. As shown in Fig. 8, the advancing contact angle reaches a steady state after these days between 99° (0.2 J/cm^2 , 70% overlap) and 118° (0.8 J/cm^2 , 80% overlap). Comparable to the θ_S steady state, increasing laser fluence and pulse overlap lead to increasing values of θ_A . It is worth to mention that laser parameters that lead to smaller θ_A directly after the surface structuring in turn lead to higher θ_A in the steady state.

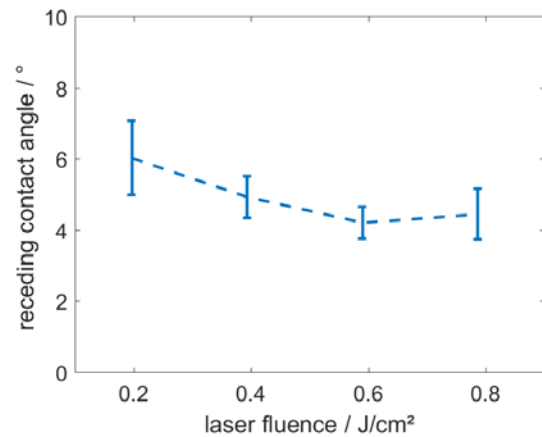


Fig. 7 Receding contact angle directly after surface functionalization as a function of the laser fluence. Error bars represent the influence of the pulse overlap.

Fig. 9 summarizes the receding contact angle in the steady state with, again, only minor influence of the laser fluence and pulse overlap. In comparison to Fig. 7, receding contact angles remain, however, below the reference value of the unstructured surface.

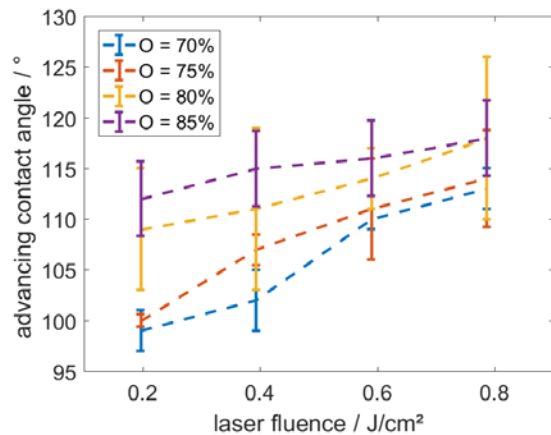


Fig. 8 Advancing contact angle 28 days after LSFL generation against laser fluence for different pulse overlap values.

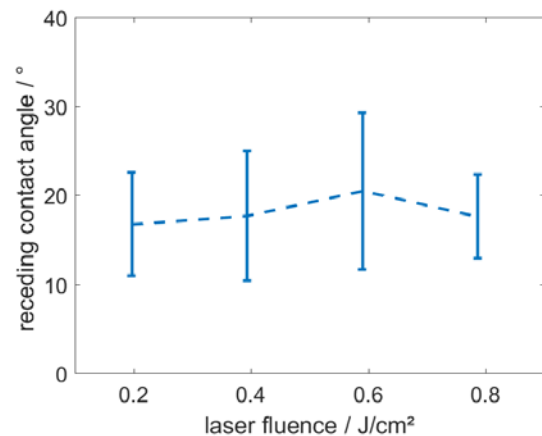


Fig. 9 Receding contact angle 28 days after surface functionalization as a function of the laser fluence. Error bars represent the influence of the pulse overlap.

The contact angle hysteresis is a calculated value using $\Delta\theta = \theta_A - \theta_R$. Measurements of θ_A and θ_R on the unstructured stainless steel surface lead to a reference value of $\Delta\theta = 56.6^\circ$. Fig. 10 depicts the contact angle hysteresis of the LSFL covered surfaces. For reasons of clarity of this diagram, the individual values of $\Delta\theta$ for different overlap values are summarized and only the mean is shown here. Directly after laser irradiation, $\Delta\theta$ decreases with increasing laser fluence from 42.3° and 20.3° . Quite the contrary, in the steady state, $\Delta\theta$ increases to values from 88.3° and 98.2° .

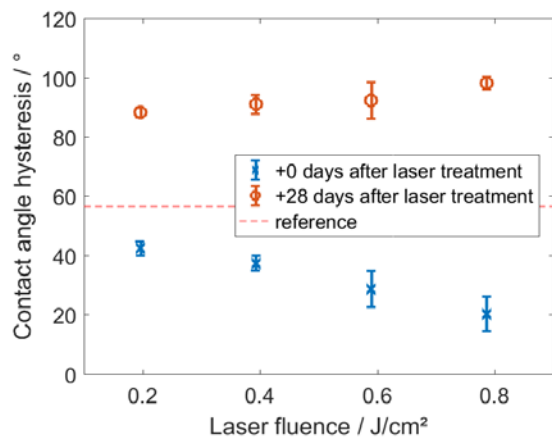


Fig. 10 Contact angle hysteresis of water on stainless steel as a function of the laser pulse energy for measurements directly after the laser irradiation (blue) and after 28 days storage time (orange). The contacts angle hysteresis for unstructured surfaces is 56.6° .

4. Conclusion

In this contribution we present comprehensive experimental results of water wetting modification by laser induced periodic surface structures on stainless steel. Laser fluence and pulse overlap are shown to complexly influence the wettability, described by the static contact angle, the advancing and receding contact angle, as well as on the contact angle hysteresis. Due to a pronounced temporal evolution of the wettability over days, the results have to be divided into 2 categories, wetting behavior directly after laser irradiation and in the steady state, here defined by 28 days after laser processing. By a sessile drop method, the static contact angle is measured, directly after the surface generation, static contact angle drops to values in the hydrophilic regime. Measurements 28 days later reveal a hydrophobic behavior with static contact angles above 97° . The dynamic wetting behavior is evaluated by the advancing and receding contact angle resulting of a sessile drop method with drop expansion and contraction. Based on these results, we find a small contact angle hysteresis directly after laser irradiation and in a big contact angle hysteresis in the steady state.

In prominent cases, high static contact angles are associated to a small contact angle hysteresis, i.e. poor wetting behavior by a droplet that slides of the surface even for a small tilt angle, e.g. lotus effect. Here, we show that LSFL covered surfaces in the steady state possesses both, a high static contact angle, i.e. a small contact area between the fluid and the solid and a high contact angle hysteresis, i.e. stable drop position on the surface. For surface engineering applications, this combination represents an intriguing opportunity for, e.g., printing and coating technologies.

References

- [1] J. Bonse, S. Höhm, S. V. Kirner, A. Rosenfeld and J. Kruger: IEEE J. Select. Topics Quantum Electron., 23, (2017) 9000615.
- [2] E. V. Golosov, V. I. Emel'yanov, A. A. Ionin, Y. R. Kolobov, S. I. Kudryashov, A. E. Ligachev, Y. N. Novoselov, L. V. Seleznev and D. V. Sinitsyn: Jetp Lett., 90, (2009) 107.
- [3] K. Okamoto, M. Hashida, Y. Miyasaka, Y. Ikuta, S. Tokita and S. Sakabe: Phys. Rev. B, 82, (2010) 165417.
- [4] J. Bonse and J. Krüger: J. Appl. Phys., 108, (2010) 34903.
- [5] F. Preusch, S. Rung and R. Hellmann: J. Laser. Micro/Nanoengin., 11, (2016) 137.
- [6] H. B. Eral, D. J. C. M. 't Mannetje and J. M. Oh: Colloid. Polym. Sci., 291, (2013) 247.
- [7] R. N. Wenzel: J. Phys. Chem., 53, (1949) 1466.
- [8] A. B. D. Cassie and S. Baxter: Trans. Faraday Soc., 40, (1944) 546.
- [9] S. Rung, S. Schwarz, B. Götzendorfer, C. Esen and R. Hellmann: Appl. Sci., 8, (2018) 700.
- [10] J. L. Ocaña, R. Jagdheesh and J. J. García-Ballesteros: Adv. Opt. Technol., 5, (2016) 87.
- [11] M. Martínez-Calderon, A. Rodríguez, A. Dias-Ponte, M. C. Morant-Miñana, M. Gómez-Aranzadi and S. M. Olaizola: Appl. Surf. Sci., 374, (2016) 81.
- [12] P. Bizi-bandoki, S. Valette, E. Audouard and S. Benayoun: Appl. Surf. Sci., 273, (2013) 399.
- [13] O. Raimbault, S. Benayoun, K. Anselme, C. Mauclair, T. Bourgade, A.-M. Kietzig, P.-L. Girard-Lauriault, S. Valette and C. Donnet: Mater. Sci. Eng. C Mater. Biol. Appl., 69, (2016) 311.
- [14] D. V. Ta, A. Dunn, T. J. Wasley, R. W. Kay, J. Stringer, P. J. Smith, C. Connaughton and J. D. Shephard: Appl. Surf. Sci., 357, (2015) 248.
- [15] H. Yan, M. R. B. Abdul Rashid, S. Y. Khew, F. Li and M. Hong: Appl. Surf. Sci., 427, (2018) 369.
- [16] M. Tang, V. Shim, Z. Y. Pan, Y. S. Choo and M. H. Hong: J. Laser. Micro/Nanoengin., 6, (2011) 6.
- [17] A.-M. Kietzig, M. Negar Mirvakili, S. Kamal, P. Englezos and S. G. Hatzikiriakos: J. Adhes. Sci. Technol., 25, (2011) 2789.
- [18] D. van Ta, A. Dunn, T. J. Wasley, J. Li, R. W. Kay, J. Stringer, P. J. Smith, E. Esenturk, C. Connaughton and J. D. Shephard: Appl. Surf. Sci., 371, (2016) 583.
- [19] S. Schwarz, S. Rung and R. Hellmann: Appl. Phys. Lett., 108, (2016) 181607.
- [20] A.-M. Kietzig, S. G. Hatzikiriakos and P. Englezos: Langmuir, 25, (2009) 4821.
- [21] I. Gnilitzkyi, T. J.-Y. Derrien, Y. Levy, N. M. Bulgakova, T. Mocek and L. Orazi: Sci. Rep., 7, (2017) 8485.

(Received: June 24, 2018, Accepted: September 9, 2018)